A computational model for color assimilation illusions and color constancy

Oguzhan Ulucan, Diclehan Ulucan, and Marc Ebner

University of Greifswald, Institute of Mathematics and Computer Science
17489 Greifswald, Germany
{oguzhan.ulucan,diclehan.ulucan,marc.ebner}@uni-greifswald.de

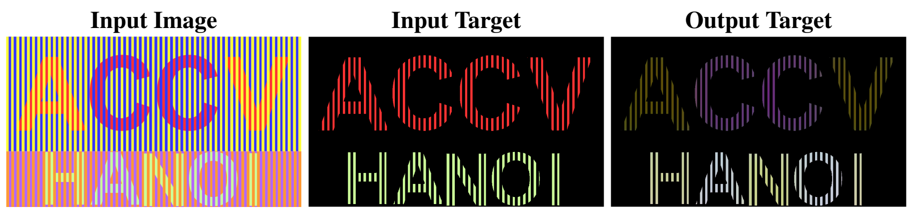

Fig. 1: Color assimilation illusion. (Left-to-right) Input image, input target's reflectance, and estimated reflectance via our method. In the input image, we perceive the colors of the letters as if they are different. However, when we remove the context as shown in the input target, we can see that the reflectances of *ACCV* and *HANOI* are the same within themselves.

Abstract. Our visual system unconsciously estimates the objects' reflectance in the scene. Even under different illumination conditions, it can *discount* the effects of the illuminant to recognize the true colors of the objects. Yet, under some circumstances, the perceived color can differ from the actual reflectance. Color illusions can be given as an example of such circumstances. While computer vision studies aim at estimating the scene's illuminant, computational biology studies mostly aim at reproducing our sensation on color illusions. However, as stated in many studies, an algorithm mimicking our perception should be deceived by color illusions, while estimating the reflectance under varying illumination conditions. Yet, to the best of our knowledge, there is no study that mimics our sensation on color illusions and also investigates computational color constancy in detail by using a single method. Based on this motivation, we develop a single method that mimics our behavior on color assimilation illusions and performs color constancy. In particular, we propose a *multiresolution color constancy* strategy that operates in scale-space. In our approach, we make use of a variant of the local space average color method which we further modify by considering the gradient changes of the scene. According to the experimental results, our algorithm mimics our sensation on color illusions, and it presents competitive results on 4 different color constancy benchmarks.

Keywords: Color illusion perception · Computational color constancy · Reflectance

1 Introduction

Color is not a physical quantity but the product of the complex mechanisms of the human brain that devotes more than 20% of its capacity to visual processing [77, 91]. One of the interesting aspects of our visual system is its ability to recognize the physical reflectance of the objects by discounting the effects of the environmental context, *i.e*., light source [17, 27, 43, 55]. This phenomenon is called as *color constancy*, and it is performed unconsciously. However, under certain circumstances, the context might deceive our visual system so that the colors we perceive can be quite different from the actual physical reflectance of the object.

We can exemplify color illusions as a circumstance where the context deceives our visual system. An example of color illusions is provided in Fig. 1. We perceive the colors of *ACCV* as purplish and orangish, and *HANOI* as yellowish and bluish, while the reflectances of *ACCV* and *HANOI* are in fact identical within themselves. This can be observed by removing the context/inducers, *i.e*., the surrounding area outside the target region, from the input image as demonstrated in the input target. The reason why we perceive the colors of the letters, *i.e*., target region, different from each other is that the context causes their colors to be shifted towards that of their local neighbors. These types of illusions are related to Munker-White illusions which can be created by placing identical gray patches, on top of black and white stripes [88, 89]. As demonstrated in the first two images in Fig. 2, even though the brightness of all gray patches is the same, we perceive them as if they are different. The reason behind this phenomenon can be explained by the *assimilation effect*. While the gray patches on top of the black stripes have more white pixels in their neighborhood, gray patches on top of the white stripes have more black neighboring pixels. This structure causes the perceived brightness of the gray patches to shift towards that of their local neighbors. Thus, we perceive the gray patches having more white neighboring pixels brighter than those with more black pixels in their neighborhood. As we present in Fig. 2, when we remove the context, we can see that the gray patches have in fact the same brightness. Furthermore, by using colored stripes and patches rather than using shades of gray we can create color assimilation illusions such as in Fig. 1 and Fig. 2. In this case, instead of the brightness of the target region, the color of it shifts towards that of its local neighbors. Consequently, locality is a crucial feature for the illusion perception, *i.e*., our perception is significantly affected by the information present in the local neighborhood of the target region.

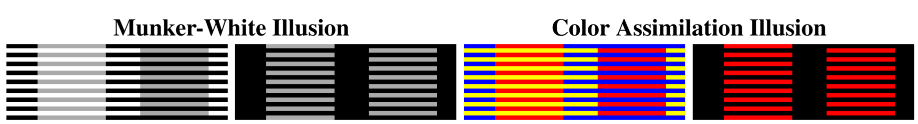

Fig. 2: Example of the Munker-White and color assimilation illusions [8]. In the Munker-White illusion, due to the assimilation effect, we perceive the gray patches on top of the black inducers brighter than the ones on top of the white inducers, although their brightness is identical. Similarly, in the color assimilation illusion, although the reflectance of the target region is red, its color shifts towards its local neighbors, hence, we perceive it as orangish and purplish.

Color constancy and color illusions are beneficial tools in the fields of computational biology [43, 74] and computer vision [50, 81]. Even though computer vision and computational biology prioritize different aspects, they both have emphasized the relationship between color illusions and color constancy [21, 51, 67, 86]. In computational biology, both phenomena are analyzed to better understand how the human visual system processes the visual information. Although myriad studies have been carried out for color constancy and color illusions, unfortunately, the exact relationship between them is still a puzzle. If this relationship could be unraveled biologically, while also explaining how our visual system performs color constancy and is fooled by color illusions, then we would obtain an accurate model of human color processing. Thus, it would be possible to design better systems for both digital photography and computer vision applications [29]. On the other hand, in computer vision, both phenomena are investigated hardly together to develop artificial systems that mimic the human visual system [51, 81]. What we find rather surprising is that in computer vision, color illusions have not been investigated in depth as color constancy although the natural link between color illusions and color constancy might provide us beneficial cues to develop algorithms that perform more accurately [51]. Only in a few recent studies, it is demonstrated that color assimilation illusions are indeed beneficial tools to improve the performance of color constancy algorithms [81, 86]. Hence, these phenomena should be further investigated together in order to understand the extent of their link's benefits. In short, while in computational biology, illusions are analyzed in detail, color constancy, *i.e.*, estimating the (shaded) reflectance by discounting the illuminant, is rather not analyzed as in computer vision. On the other hand, in computer vision, illuminant estimation is widely studied, yet color illusions are rarely considered. However, as pointed out in computational biology, a method designed for mimicking our perception should be deceived by color illusions and perform color constancy together [21].

In this paper, we aim at developing a single method that can both reproduce our sensation on color illusions and perform color constancy. In other words, we design an algorithm that solves both phenomena without focusing on developing a method explicitly for one phenomenon or other. To design a single method we combine the best of two worlds, *i.e.*, we consider the observations provided in computational biology while also benefiting from the ability of estimating the illuminant as performed in computer vision studies. We develop a method that relies on low-level processing, in particular, to scale-space representations, and space average color which can be obtained by using spatial filters, based on the following observations in human color processing. Firstly, the information we require for illumination estimation is available in the stimulus at the proper scale [74, 75]. Secondly, the global changes caused by the illuminant are essentially carried in the low spatial frequency component, hence removing the blurry content from the image can provide us an output similar to our perception [24, 74, 75]. Finally, the human visual system might be discounting the illuminant based on space average color [18, 27, 64], which is also explicitly demonstrated in Land's experiments [61].

There exist several methods/investigations that try to mimic our perception of illusions [13, 21, 50, 51, 53, 59, 66, 67, 69, 81, 92]. Algorithms performing low-level processing for mimicking our sensation on illusions mostly utilize a set of spatial filters such as exponential filters [92], or oriented difference of Gaussians/Laplacians at multiple scales [13, 73]. These algorithms usually consider the lightness/brightness illusions, *i.e.*, the Munker-White illusion, and they do not provide explicit investigations on computational color constancy as we do in our study. The studies that are most similar to our algorithm are the ones that use spatial filters. However, as aforementioned, these methods only aim at reproducing our perception of illusions. Also, most of these methods provide the results of the spatial filters as their final outputs, while we aim to produce an output image with the same algorithmic process for both the illusions and color constancy.

It is important to mention that we do not suggest that our approach is a perfect model of the human visual system whose mechanisms have not been fully discovered yet. In other words, we are not arguing that our algorithm does carry out the exact operations performed by the human visual system. We only aim to develop a method for computational color constancy and the perception of color assimilation illusions from the perspective of computer vision. To the best of our knowledge, this is the first color constancy study that solves both phenomena together while providing an analysis of color constancy from the perspective of computer vision.

The remainder of this paper is organized as follows. In Sec. 2, we provide a general overview of image formation and color constancy. In Sec. 3, we revisit the local space average color algorithm and introduce our method. Then, in Sec. 4 we discuss our results for color illusions, and in Sec. 5 we demonstrate the efficiency of our algorithm on color constancy. Afterwards, in Sec. 6 we provide a summary of our study.

2 Image Formation Model and Computational Color Constancy

Before introducing our algorithm we would like to provide a brief summary of the commonly used image formation model in the field of color constancy since we conduct our investigations from the perspective of computational color constancy.

We begin visual information processing when the light falls onto the retina where it is measured by the photoreceptors, *i.e.*, cones, while cameras begin visual information processing when a sensor array measures the incident light. If we assume that we have a camera consisting of three different sensors, then each sensor measures the energy of the incident light by responding to a specific part of the visible spectrum, *i.e.*, short-, middle-, and long-wavelength. As a result, for every spatial location (x, y) the measured signal $I(x, y)$ depends on the irradiance $E(x, y)$ hitting the sensors of the camera and the sensor sensitivity function S of the capturing device containing the sensors responses of a specific wavelength. Thus, we can model the measured signal as follows:

$$I(x, y) = \int_w E(x, y; \lambda) S_i(\lambda) d\lambda, \tag{1}$$

where $i \in \{\text{long, middle, short}\}$, and λ is the wavelength of the visible spectrum w.

In color constancy, we mostly build our methods upon two assumptions; *(i)* the surface is Lambartian, *i.e.*, it is equally reflecting the light into all directions, and *(ii)* there is a point light source $L(x, y; \lambda)$ illuminating the scene. Based on these assumptions, the irradiance hitting the sensors of the camera can be formulated as follows:

$$E(x, y; \lambda) = G(x, y) R(x, y; \lambda) L(x, y; \lambda), \tag{2}$$

where $R(x, y; \lambda)$ is the reflectance, and $G(x, y)$ is the scaling factor which can be represented as $cos\ \alpha$, where α is the angle between the surface normal vector and a vector pointing in the direction of the light source. Thus, by using Eq. (1) and Eq. (2) we can model an image as follows:

$$I(x, y) = G(x, y) \int_w R(x, y; \lambda) L(x, y; \lambda) S_i(\lambda) d\lambda. \tag{3}$$

In computational color constancy, we aim at estimating the illuminant L from the color cast image I in order to produce a canonical image, *i.e.*, a white-balanced image. However, even when we simplify the image formation model and represent it as in Eq. (3), color constancy remains an under-constrained problem since the number of unknown elements is higher than the number of known components. In order to overcome the ill-posed nature of color constancy, generally relaxations are made by assuming that the scene is illuminated by a single light source, the camera sensor responses are narrow-band, *i.e.*, they can be approximated by Dirac's delta functions, and the scene geometry $G(x, y)$ has no impact on the illumination estimation task [27]. With these oversimplifications, a color cast image is assumed to be scaled by a uniform light source, and it is represented as the element-wise product of the (shaded) reflectance R and the global light source $\mathbf{L}$ as follows:

$$I(x, y) = R(x, y) \odot \mathbf{L}. \tag{4}$$

Over the last decades, numerous global color constancy algorithms have been proposed to estimate the color vector of the light source [27]. These algorithms can be simply grouped into two categories, namely, traditional methods and data-driven models. Traditional methods make use of image statistics, and there are two well-known traditional algorithms, *i.e.*, white-patch Retinex and gray world [18, 62]. The former takes into account that the human visual system might be discounting the illuminant based on the highest luminance patch and estimates the illuminant by computing the maximum responses of the image channels separately [62]. The latter considers that the scene's space-average color is crucial for human color constancy and takes the mean of the pixels of each image channel individually [18]. Since these two methods are developed based on investigations of the human visual system and it is known that methods based on biological findings have a tendency to perform effectively, these two algorithms lay the foundations of several other color constancy studies [20, 35, 46, 57, 71, 72, 83, 84, 87]. Indeed, there are also other traditional color constancy approaches that mimic different mechanisms of the human visual system to discount the illuminant of the scene [39, 41, 42, 81, 93].

Even though traditional methods are cost-efficient, their accuracy in estimating the illuminant is not sufficient in case a limited number of distinct colors is present in the scene, *i.e.*, scenes with close-up shootings or with dominant sky/grass regions [19]. On the other hand, data-driven methods can usually achieve high performance when uniformly colored areas dominate the scene. Examples of data-driven algorithms include diverse strategies such as gamut-based methods [12, 33, 34, 36, 47], Bayesian approaches [15, 16, 45], and neural network-based models [1, 11, 22, 25, 54, 60]. While data-driven models generally outperform traditional algorithms on well-known benchmarks, their performance tends to decrease when they are tested on scenes with out-of-ordinary statistical distributions and/or scenes captured by cameras with unknown characteristics [40, 71, 82]. The decrease in their effectiveness can be explained by the facts that *(i)* data-driven methods expect similar training and test sets, *(ii)* well-known benchmarks contain similar lighting conditions, *i.e*., illuminants on the edges and outside the color temperature curve are rarely included, and *(iii)* most datasets are formed with capturing devices having similar sensor response specifications [19, 82].

The majority of traditional and data-driven methods previously exemplified tackle the ill-posed problem by assuming that there is a single illuminant in the scene. Although, this assumption allows us to produce visually pleasing images, it is usually violated in the real world due to the presence of interreflections, shadows, and multiple light sources in the scene [14, 29]. In case multiple illuminants are present in the scene, the image formation model given in Eq. (1) can be rewritten as follows [32]:

$$I(x,y) = \int_w \sum_{j=1}^{n} \beta_j(x,y) E_j(x,y;\lambda) S_i(\lambda) d\lambda, \tag{5}$$

where n is the number of illuminants, and $\beta \in R^+$ is the weighting factor, which depends on the intensities of the light sources and the scene's geometry.

Compared to the global color constancy algorithms, the number of multi-illuminant color constancy methods is quite limited. One of the earliest attempts to produce pixel-wise estimates of the light source is the local space average color algorithm created by Ebner [26]. Afterwards, several methods have been developed that rely on both traditional and data-driven strategies [7, 9, 11, 22, 41, 49, 56, 85, 93].

3 Method

As aforementioned in Sec. 1, our simple yet effective approach relying on low-level processing can produce output images for both color assimilation illusions and color constancy. In this section, we first revisit the local space average color [26], and then we introduce our approach.

3.1 Revisiting Local Space Average Color

We use the local space average color algorithm proposed by Ebner [26] that relies purely on low-level processing and has several connections with the human visual system. In this section, we briefly mention the reasons that led us to consider this algorithm in our approach, and then we explain the algorithm while presenting our modification.

Both in behavioral experiments and computational biology studies it is shown that local space average color might be used in the human visual system since local contrasts between neighboring cones carry important cues for human color constancy [37, 44, 79], while it is discussed in detail that space average color over a large local area is another cue for color constancy and color perception [26, 44, 64]. Also, the importance of the interaction between local spaces in color perception is explicitly demonstrated in Land's experiments where it is shown that our visual system processes the color information of the object by taking the surroundings into account [61]. Land demonstrated that when a single green or yellow patch of a Mondrian image is observed in isolation/void mode, the color of the patch is perceived as grayish-white. However, when the surrounding patches are added, *i.e.*, the Mondrian is viewed as a whole, the actual reflectance of the green or yellow patch can be observed. Due to its biological basis, and being a learning-free multi-illuminant color constancy algorithm that relies on low-level processing, we utilized local space average color in our approach.

The local space average color algorithm assumes that the effects of the light source are spatially varying. It estimates the colors of the illuminant present in the scene by iteratively updating the following equations:

$$a'_i(x,y) = \frac{1}{\mid N(x,y) \mid} \sum_{(x',y') \in N(x,y)} a_i(x',y') \tag{6}$$

$$a_i(x,y) = I_i(x,y)p + a'_i(x,y)(1-p), \tag{7}$$

where a is the space average color, N is the set of neighborhood pixels, p is the parameter that adjusts the size of the region where the local space average color is computed, *i.e.*, a small p value indicates that local space average color is computed for a large region, and subscript i represents the color channels of the image, $i \in \{r, g, b\}$.

Even though iteratively updating a_i over time allows us to estimate the illuminant, convergence may take time which increases the computational cost of the algorithm. Therefore, the simplest way to reduce the run-time while obtaining similar results is to replace the iterative approach with a convolution operation as follows:

$$a_i(x,y) = k(x,y) \int\int I_i(x,y) g(x-x', y-y') dx' dy', \tag{8}$$

where the scaling factor k is chosen such that

$$k(x,y) \int\int I_i(x,y) g(x', y') dx' dy' = 1, \tag{9}$$

where g is the 2D Gaussian kernel formulated as $g(x,y;\sigma) = \frac{1}{2\pi\sigma^2} exp(-\frac{x^2+y^2}{2\sigma^2})$, σ is the controlling parameter of the Gaussian kernel that is usually set to a constant such as $\sigma = \gamma\ (max\{h, w\}/2)$ where h and w are the height and width of the image, respectively. The γ parameter has to be selected such that local averaging can be performed over a sufficient area that contains different objects with diverse reflectances. The reason is that the local space average color algorithm assumes that the world is achromatic on average and this hypothesis is only valid when there is a sufficient number of diverse colors present in the scene [27]. According to practical experiments, setting γ to 0.95 for single illuminant cases and 0.095 for the multi illuminant cases produces satisfying results. Therefore, γ can be assigned to a value between 0.095 and 0.95 according to the illumination conditions of the scene, *i.e.*, for single illumination conditions, γ should be chosen larger, whereas, for mixed illumination conditions, it should be smaller.

After obtaining a, the input's (shaded) reflectance o can be obtained as follows:

$$o(x,y) \approx \frac{I(x,y)}{fa(x,y)}, \tag{10}$$

where f is a factor that scales all color channels equally and it is assigned to 2 assuming a perpendicular orientation between the object and the camera [27].

In 2013, Ebner and Hansen [30] demonstrated a variant of the algorithm where the local averaging is performed according to the depth information of the scene. The main idea is built upon the fact that separate objects present in the scene may cause large depth discontinuities. Thus, areas divided by the large depth differences should be treated separately when estimating the illuminant. One of the main drawbacks of this algorithm is that the depth information might not be easily accessible, and the range data might be noisy which may severely affect the calculation of the estimates. Therefore, we follow the main idea of the prior work, but instead of relying on depth information, we utilize the gradients of the scene since it is known that large depth discontinuities cause large gradient changes [90]. To respect the edges and preserve the coherence of the local information [28], we refine the local estimates by using an edge-aware smoothing filter [52]. Since guided filtering assumes that the processed image is locally a linear transform of the guidance image [52], this post-processing step helps us to respect gradient changes in the local estimates according to the input image.

3.2 Proposed Algorithm

Our method reconciles two computationally opposing perceptual phenomena, *i.e.*, it obtains canonical images from scenes with a color cast and it is deceived by color assimilation illusions. As aforementioned, our algorithm relies on computations in scale-space and the local space average color method modified with an edge-aware smoothing filter. We perform operations in scale-space since the information we need for accurate local estimates is available in the stimulus at the proper scale [74, 75]. We discount the effects of the blurry content from the input at each scale to obtain an output similar to our perception since it is known that the changes arising from the context are carried in the low spatial frequency element and removing the blurry content from the input can generate images similar to our perception [24, 74, 75]. In the remainder of this section, we introduce our algorithm step-by-step.

We apply preprocessing in case an sRGB image and/or a natural scene is given as input to our algorithm. For the former, we apply gamma correction to obtain a linear relationship between pixels [27], where it is worth mentioning that this is an oversimplification neglecting the non-linearity introduced by most cameras before producing the final sRGB images [2]. For the latter, we remove the 3% of the darkest and the brightest pixels to reduce possible noise since natural scenes may contain saturated pixels.

Afterwards, we obtain a lightness layer. Lightness is the visual perception of the luminance and our visual system adapts to the luminance in our surroundings by maximizing the response range available to itself [74]. If we map this adaptation to computer vision it can be explained as adjusting the statistical distribution of a certain dimension of an image so that the number of levels that can be differentiated along that certain dimension is maximized. The lightness adaptation in the human visual system can be mimicked by histogram equalization in computer vision [74]. Based on this observation, to mimic the behavior of our visual system, *i.e.*, to adjust the scene's perceived luminance, we extract a *lightness layer* from the (preprocessed) input image. To obtain the lightness layer, we take the mean of each color channel individually and scale the input image according to these values, *i.e.*, we apply the gray world algorithm [18]. Then, we convert the scaled RGB image into CIELAB color space by using $D65$ as white point, while in our experiments we observed that utilizing other white points has negligible impact on the results. Subsequently, we extract the lightness component L^*, and we perform histogram equalization [94] on L^* to adjust its contrast and utilize the resulting image as our lightness layer at the end of our process.

Then, in order to perform operations in scale-space we create two image pyramids. We form one image pyramid for the input image and one for the local estimations. We determine the number of the pyramids' scales M based on the image resolution as $M = \lfloor log(min(h,w))/log(2) \rfloor - 2$ where h and w are the height and width of the image. The last two coarsest layers are discarded due to the significant degradation of locality at these layers. Subsequently, we find the representations of the input image at multiple levels in the image pyramid. Afterwards, we utilize the local space average color algorithm explained in Sec. 3.1 to find the local estimates of the scene for each pyramid level. It is worth mentioning that we compute the local space average color at each scale separately rather than computing it only at the finest scale and then carry this estimation into scale-space. We follow this approach to preserve the fine details in the estimations at each scale more accurately. If we would compute the local space average color only at the finest level and carry these estimations into scale-space we would distort locality through downsampling, which we would like to avoid since locality is critical in particular for assimilation illusions and multi-illuminant color constancy (visual investigations are provided in the supplementary material).

After we form the scale-space representations of the input image and the local estimates, we perform an operation that we call *multiresolution color constancy* for which we take inspiration from the study of Mertens *et al*. [68]. Their method is widely utilized in the field of image fusion, where the output image is obtained by weighted averaging multiple images with their corresponding weight maps. In their strategy, the Laplacian pyramid of the input images and the Gaussian pyramid of the corresponding weights are computed. Fusion is carried out at each scale and then the resulting pyramid is collapsed into an output image. This multiresolution blending approach allows the preservation of both the fine details and the structure of flat regions in the fused images. Motivated by this idea, we propose a multiresolution color constancy strategy that can both produce white-balanced images and mimic our sensation on color assimilation illusions. In our case, we do not have multiple input images but one pyramid for the input images and one pyramid for its local estimations (see illustration in the supplementary material).

Let us explain our strategy by considering the input image and its local estimates at the m-th scale of both pyramids, where $m \in M$. We form the Laplacian pyramid of the input image $\mathcal{L}\{I_m(x,y)\}$ and the Gaussian pyramid of the local estimates $\mathcal{G}\{a_m(x,y)\}$, where the number of levels T is computed according to the image resolution as explained before. Then, we estimate the (shaded) reflectance at a scale t by applying a similar operation to Eq. (10) as follows:

$$\mathcal{P}\{o_m(x,y)\}^t = \frac{\mathcal{L}\{I_m(x,y)\}^t}{\mathcal{G}\{a_m(x,y)\}^t}, \quad t = 1,2,\dots,T, \tag{11}$$

where we form the resulting pyramid $\mathcal{P}\{o_m(x,y)\}$ by repeating this operation for all levels in T.

Subsequently, we collapse the pyramid $\mathcal{P}\{o_m(x,y)\}$ to obtain a final output for the m-th scale. To collapse $\mathcal{P}\{o_m(x,y)\}$, we first upsample the image in the coarsest scale to match the size of the image in the consecutive finer level as follows:

$$U' = upsample(\mathcal{P}\{o_m(x,y)\}^T, size(\mathcal{P}\{o_m(x,y)\}^{T-1})), \tag{12}$$

where U' is the upsampled image, $upsample$ is a function that matches the size of $\mathcal{P}\{o_m(x,y)\}^T$ to the size of $\mathcal{P}\{o_m(x,y)\}^{T-1}$.

After obtaining U', we linearly combine it with the image on the consecutive finer level as follows:

$$U = average(U', \mathcal{P}\{o_m(x,y)\}^{T-1}), \tag{13}$$

where U is the new image at the level $T-1$, and $average$ represents the linear combination operation.

Afterwards, we upsample U to linearly combine it with its consecutive finer level $T-2$. We perform Eq. (12) and Eq. (13) until we reach the finest level of the pyramid. The computed image at the finest scale represents the estimated reflectance for the m-th scale. We repeat this procedure for all $m \in M$.

Then, we collapse the resulting pyramid for the estimated reflectances by utilizing Eq. (12) and Eq. (13). The resulting image is the (shaded) reflectance of the input image.

This method allows us to perform two computationally opposing perceptual phenomena with a single method. If we would not adopt such a strategy, and directly divide the input image with its local estimations only on a single scale, we could not reproduce our sensation on color illusions, even though we would be able to perform color constancy (a brief explanation is provided in the supplementary material).

Lastly, in order to obtain the final output image, we apply the following procedure. We convert the estimated reflectance image into CIELAB color space and take the a^* and b^* channels. Then, we merge these channels with the previously extracted lightness layer. Subsequently, we convert the resulting image into RGB color space and obtain our final output image.

4 Results on Color Illusions

In this section, first we explain how we form our color illusion set, and then we provide our analysis of color illusions.

As explained in Sec. 1, we are deceived by color assimilation illusions due to the influence of the context, *i.e.*, inducers [70]. The frequency of occurrence of the inducer and its thickness control the strength of the illusion effect (an example demonstration for the effects of the context is provided in the supplementary material). Hence, we form our color illusion set by taking the inducer's frequency of occurrence and its thickness into account. We choose different shapes for the target region while we select various colors for both the context and the target area. As a result, we form an illusion set that includes a range of images that begin to evoke an illusion effect to images with a strong illusion sensation (example images of illusions are provided in the supplementary material). It is worth mentioning that the images created by ourselves are available upon request [80].

In order to evaluate an algorithm's performance on reproducing our sensation on color illusions, there are two common approaches; *(i)* conducting visual analysis of the target region, and *(ii)* presenting the intensity change within the target area. Neither of these two approaches includes a quantitative analysis since there is no error metric designed for this task and there is no color assimilation illusion dataset including ground truth information. The lack of metrics and datasets can be considered among the challenges/limitations in this field. Creating an error metric and an illusion dataset are troublesome tasks since even if we consider only observers with normal vision, the sensory processing of individuals varies from each other [31, 78], thus they may not perceive a color illusion entirely the same. For instance, even if different observers perceive a target area as green, the perceived shade of green may be different among the observers, which is the reason behind providing the intensity change within the target image or performing visual inspections in several studies reproducing our sensation on color illusions [21, 38, 67]. In this study, to investigate the performance of our algorithm in mimicking our sensation on color assimilation illusions, we prefer to carry out a visual inspection by considering the target regions of the images.

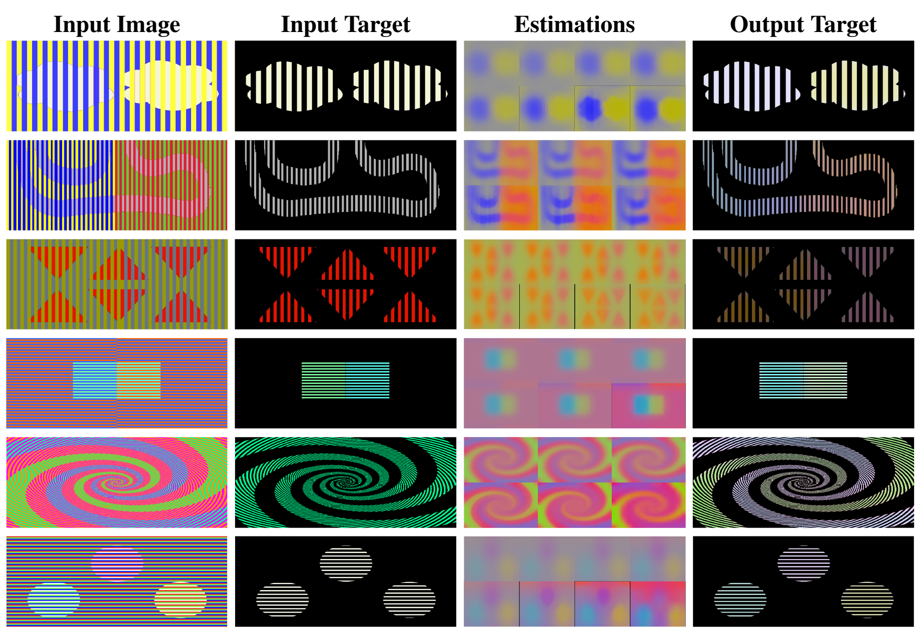

Fig. 3: Results of the proposed method on color illusions. When we look at the input images, we perceive their target regions as if they have different colors. However, as demonstrated in the images in second column, they have the same color. As shown in the output's target regions, our method mimics our perception of color illusions having different inducer frequencies/thicknesses, colors, and shapes. Note that, the colors in the output target may seem darker than our perception in the input image due to the black background in the output target. The images in the first three rows are our designs, while the subsequent rows contain images courtesy of David Novick, Akiyoshi Kitaoka, and Michael Bach, respectively.

We would like to note that while we cannot measure our sensation quantitatively, as a close alternative, to present quantitative analysis one might perform experiments similar to color-matching experiments with human observers having normal color vision, *i.e.*, without any color deficiency [86]. In such an experiment, one may ask the observers to match the colors of the target region with a patch whose RGB values can be adjusted by the observers. Consequently, in the end, we can obtain ground truth RGB values of the target region which we can utilize to carry out quantitative analysis to evaluate the algorithms mimicking our sensation on color illusions. Nonetheless, due to constraints in technical capacity and resource availability, creating a benchmark for color assimilation illusions including ground truths by conducting experiments with human observers is deemed to be beyond the scope of our study.

We demonstrate our results on various color illusions containing different shapes, and color combinations in Fig. 3 (for further visual results, please refer to the supplementary material). We provide both our estimations at different scales and the output targets. As we can see, our algorithm can mimic our sensation on various color illusions.

It is worth mentioning that in our recent study [86], we considered the pixel-wise estimations of the modified color constancy algorithms as the reproduction of our sensation on color illusions. We mentioned that the reproduction of illusions is highly dependent on the inducer's frequency of occurrence and thickness. While this dependency is valid for algorithms operating on a single scale, it can be overcome by a scale-space approach as we propose in this work. This can be explained by the fact that even if the parameter for spatial filtering is insufficient for the finer scales, it is adequate for the coarser scales. Since our multiresolution color constancy strategy allows us to consider multiple scales, we can give more importance to the coarser scales where the illusion sensation is stronger. Hence, when we collapse the pyramid we can produce results that are close to our perception of assimilation illusions without relying on explicit parameters for the inducer's frequency of occurrence and thickness. This outcome can be associated with the fact that as the information we need for accurately estimating the illuminant is available in the stimulus at the proper scale [74, 75], the information we need to reproduce the color illusions might also be available at the proper scale. This would also indicate that there is a strong relationship between color assimilation illusions and color constancy which should not be neglected and further investigated.

5 Results on Color Constancy

In this section, we explain our experimental setup and provide statistical results. Detailed information about the datasets and error metrics, as well as visual results, can be found in the supplementary material.

To evaluate the performance of our method, we utilize the angular error and the $\triangle$E metric [65, 76], and we use 4 different datasets, namely, the Multiple Illuminant and Multiple Object (MIMO) dataset [9], the Mixed-Illumination Test Set [4], the Rendered WB Dataset (Set 2) [6], and the rendered version of the Cube+ [6].

To provide consistent results with other studies that we utilized for comparison we report the mean and second quartile (Q2) of the angular error for the MIMO dataset,

Table 1: Statistical results on 4 benchmarks. The results are reported based on the recent publications of Ulucan *et al*. [86], Kinli *et al*. [58], and Afifi *et al*. [6]. The top results are highlighted by using color coding as, the best: green, second-best: blue, and third-best: red. AC and AT are the auto-color and auto-tone functions of Adobe Photoshop, respectively.

	MIMO Dataset	Real-World Mean	Real-World Q2	Laboratory Mean	Laboratory Q2
Single-Illuminant Methods	White-Patch Retinex [63]	6.8°	5.7°	7.8°	7.6°
	Gray World [18]	5.3°	4.3°	3.5°	2.9°
	Shades of Gray [35]	6.2°	3.7°	4.9°	4.6°
	1^{st} - Gray Edge [87]	8.0°	4.7°	4.3°	4.1°
	Weighted Gray Edge [48]	7.9°	4.1°	4.4°	4.0°
	Mean Shifted Gray Pixels [72]	5.8°	5.0°	13.3°	12.6°
	Block-based Color Constancy [83]	4.8°	3.6°	3.1°	2.8°
	Biologically Inspired Color Constancy [81]	5.0°	4.3°	4.2°	4.1°
	Color Constancy Convolutional Autoencoder [60]	12.4°	12.3°	13.9°	14.1°
	Sensor-Independent Color Constancy [2]	5.9°	5.1°	9.0°	9.0°
	Cross-Camera Convolutional Color Constancy [1]	11.9°	13.0°	7.0°	7.1°
Multi-Illuminant Methods	Local Space Average Color [26]	4.9°	4.2°	3.1°	3.0°
	Gijsenij *et al*. with White-Patch Retinex [49]	4.2°	3.8°	5.1°	4.2°
	Gijsenij *et al*. with Gray-World [49]	4.4°	4.3°	6.4°	5.9°
	Conditional Random Fields with White-Patch Retinex [9]	4.1°	3.3°	3.0°	2.8°
	Conditional Random Fields with Gray-World [9]	3.7°	3.4°	3.1°	2.8°
	N-White Balancing with White-Patch Retinex [7]	4.1°	3.4°	2.6°	2.2°
	N-White Balancing with Gray World [7]	4.6°	4.5°	3.7°	3.1°
	Visual Mechanism based Color Constancy with Bottom-Up [41]	5.0°	4.0°	3.7°	3.4°
	Retinal Inspired Color Constancy [93]	5.2°	4.3°	3.2°	2.7°
	Color Constancy Adjustment based on Texture of Image [56]	3.8°	3.8°	2.6°	2.6°
	Gray Pixels with 2 clusters [71]	3.7°	3.3°	3.0°	2.5°
	Gray Pixels with 4 clusters [71]	3.9°	3.4°	2.7°	2.2°
	CNNs-based Color Constancy [11]	3.3°	3.1°	2.3°	2.2°
	GAN-based Color Constancy [22]	3.5°	2.9°	-	-
	Proposed	3.2°	2.6°	2.7°	2.3°

	Angular Error				△E 2000 [76]			
Rendered Mixed-Illumination Test Set	Mean	Q1	Q2	Q3	Mean	Q1	Q2	Q3
Local Space Average Color [26]	4.8°	3.3°	4.6°	8.1°	11.0	8.1	10.4	14.7
Gray Pixels [72]	19.7°	11.9°	17.2°	27.1°	25.1	19.1	22.6	27.5
Grayness Index [71]	6.4°	4.7°	5.7°	7.1°	12.8	9.6	12.5	14.6
KNN White-Balance [6]	5.8°	4.3°	5.8°	6.9°	12.0	9.4	11.6	13.6
Interactive White-Balance [5]	5.9°	4.6°	5.6°	6.6°	11.4	8.9	10.9	12.8
Deep White-Balance [3]	4.5°	3.6°	4.2°	5.2°	10.9	8.6	9.8	12.0
Auto White-Balance for Mixed-Scenes [4]	5.4°	4.3°	4.9°	6.2°	10.6	9.4	10.7	11.8
Style White-Balance [58]	5.7°	4.5°	5.4°	6.3°	12.1	10.4	12.1	13.4
Proposed	4.8°	3.4°	4.4°	6.3°	8.9	6.7	8.5	12.0

	Angular Error				△E 2000 [76]			
Rendered WB Dataset (Set 2)	Mean	Q1	Q2	Q3	Mean	Q1	Q2	Q3
Local Space Average Color [26]	8.7°	4.3°	8.0°	14.2°	10.6	6.6	10.3	15.2
Adobe Photoshop (AC) [23]	10.2°	5.3°	8.6°	14.1°	11.7	7.6	11.4	15.0
Adobe Photoshop (AT) [23]	11.9°	7.0°	10.7°	15.9°	13.1	9.6	13.2	16.5
White-Patch Retinex [63]	13.2°	8.2°	12.6°	18.1°	12.9	9.0	13.4	17.1
Gray World [18]	8.6°	5.4°	7.9°	10.9°	10.7	7.7	10.1	13.2
Shades of Gray [35]	9.0°	5.3°	8.3°	12.0°	9.8	6.9	9.7	12.5
1^{st} - Gray Edge [87]	12.5°	7.6°	11.9°	17.0°	13.0	9.1	12.9	16.6
2^{nd} - Gray Edge [87]	12.8°	7.6°	12.1°	17.5°	13.2	9.0	13.1	17.0
Weighted Gray Edge [48]	13.5°	7.8°	12.6°	18.6°	14.0	9.0	13.7	18.6
Fully Convolutional Color Constancy [54]	10.4°	5.3°	9.3°	14.2°	10.8	7.4	10.6	13.8
Quasi-Unsupervised Color Constancy [10]	10.5°	5.9°	9.4°	14.0°	10.7	7.0	10.5	13.9
WB-sRGB [6]	4.5°	2.3°	3.6°	6.0°	5.6	3.4	4.9	7.1
Proposed	7.8°	3.7°	7.1°	12.9°	10.3	6.1	10.0	15.2

	Angular Error				△E 2000 [76]			
Rendered Cube+	Mean	Q1	Q2	Q3	Mean	Q1	Q2	Q3
Local Space Average Color [26]	6.1°	2.2°	5.3°	11.4°	8.6	4.4	8.0	13.8
White-Patch Retinex [63]	8.4°	2.2°	5.0°	13.2°	14.2	3.9	8.5	22.7
Gray World [18]	6.4°	2.5°	5.1°	9.1°	8.1	4.2	7.3	11.1
Shades of Gray [35]	6.7°	2.1°	4.2°	9.6°	7.6	3.0	5.7	11.1
1^{st} - Gray Edge [87]	7.3°	2.1°	4.4°	10.8°	8.2	3.0	5.8	12.4
2^{nd} - Gray Edge [87]	7.2°	2.1°	4.3°	10.6°	8.1	3.1	5.6	12.1
Weighted Gray Edge [48]	7.3°	2.0°	4.2°	10.6°	8.2	2.9	5.5	12.3
Fully Convolutional Color Constancy [54]	6.5°	3.3°	5.6°	8.6°	10.4	6.6	9.8	13.3
Quasi-Unsupervised Color Constancy [10]	6.1°	2.0°	3.9°	8.8°	7.3	2.9	5.2	10.4
WB-sRGB [6]	4.1°	2.0°	3.2°	5.0°	5.7	3.2	4.6	6.7
Proposed	5.5°	1.8°	4.7°	10.6°	8.3	3.9	7.7	13.8

while we provide the mean, first quartile (Q1), second quartile, and third quartile (Q3) of both the angular error and △E 2000 for other datasets.

Table 1 presents the statistical results on all benchmarks. In terms of mean angular error, our approach is always among the three best-performing methods. Also, our learning-free algorithm presents competitive results compared to the state-of-the-art learning-based models, and it even outperforms some of them on different benchmarks.

For the MIMO dataset, our method achieves the best mean and Q2 of the angular error on the Real-World set, while it is among the three best-performing methods on the Laboratory set. Our statistical scores are slightly better on the Laboratory set which can be explained by the fact that the scenes in this set do not contain as much complexity as the ones in the Real-World set as also reported in other studies [71].

Additionally, we present results on three benchmarks that feature a higher number of outdoor scenes, as well as more diverse and challenging illumination conditions, compared to the MIMO dataset. As demonstrated in Tab. 1, on the Mixed-Illumination Test Set, our method presents the best mean, Q1, and Q2 △E scores, while it achieves state-of-the-art performance in terms of angular error. Moreover, our algorithm achieves competitive results on the Rendered WB Dataset (Set 2) and the Rendered Cube+ datasets. Overall, the data-driven WB-sRGB model presents the best scores for the Rendered WB Dataset, while we achieve the second-best results in terms of angular error. These results highlight the effectiveness of our approach across various benchmarks and challenging illumination conditions.

As a final note, based on the statistical outcomes, we may argue that the relationship between the color assimilation illusions and color constancy should be further investigated since with a single learning-free algorithm based on low-level processing we can both reproduce the color illusions and perform color constancy efficiently. Furthermore, if we can successfully both mimic our sensation on color illusions and perform color constancy with a simple yet effective learning-free approach, we may achieve even better outcomes, in particular in terms of color constancy, if we design a neural network-based model. Through the learning process, the model may adjust its parameters more accurately than traditional methods. Furthermore, in case we train the model with color illusions that are independent of sensor characteristics of the camera, we might be able to prevent the data bias arising due to the capturing device's specifications and the illumination type [19, 82]. Consequently, we might develop more robust artificial models mimicking the human visual system by minutely investigating color illusions from the perspective of computational color constancy.

6 Conclusion

The human visual system can discount the illuminant and recognize the actual physical reflectance of objects, yet under certain circumstances it cannot identify the true colors in a scene. Color illusions can be given as an example where our visual system is deceived by the context. While both discounting the illuminant and being fooled by color illusions are the result of the unknown mechanisms of our visual system, we do not exactly know how we perform color constancy, and why we are fooled by the color illusions. What we do know is that there is a relationship between these phenomena and a perfect algorithm mimicking our visual system should both reproduce our sensation on color illusions and perform color constancy. If we design an approach that can respond to both phenomena, it would help to uncover the mechanisms of the human visual system. From this motivation, we have developed a single method that can both reproduce our sensation on color illusions and perform color constancy by making use of observations provided in numerous computational biology and computer vision studies. Our multiresolution color constancy strategy where we utilize scale-space within scale-space allows us to address both phenomena through a single method. It enables us to perform color constancy since we discount the illuminant at each scale, while it allows us to mimic our sensation on illusions since we take the information at the coarser levels where the illusion effect is stronger into account.

As future work, we will use our observations from our algorithm to analyze color illusions from the perspective of learning-based color constancy models. Moreover, we will focus on one of the challenges of the field, i.e., lack of evaluation benchmarks, by creating a color assimilation illusion benchmark.

Acknowledgments. The authors would like to thank Michael Bach, Akiyoshi Kitaoka, and David Novick for giving permission to use their color illusions.

Disclosure of Interests. The authors have no competing interests to declare that are relevant to the content of this work.

References

1. Afifi, M., Barron, J.T., LeGendre, C., Tsai, Y.T., Bleibel, F.: Cross-camera convolutional color constancy. In: IEEE/CVF Int. Conf. Comput. Vision. pp. 1981–1990 (2021)
2. Afifi, M., Brown, M.S.: Sensor-independent illumination estimation for DNN models. In: Brit. Mach. Vision Conf. BMVA Press (2019)
3. Afifi, M., Brown, M.S.: Deep white-balance editing. In: IEEE/CVF Conf. Comput. Vis. Pattern Recog. pp. 1397–1406 (2020)
4. Afifi, M., Brubaker, M.A., Brown, M.S.: Auto white-balance correction for mixed-illuminant scenes. In: IEEE/CVF Winter Conf. Appl. Comput. Vision. pp. 1210–1219 (2022)
5. Afifi, M., Brown, M.S.: Interactive white balancing for camera-rendered images. In: Color Imag. Conf. vol. 28, pp. 136–141. Soc. Imag. Sci. Technol. (2020)
6. Afifi, M., Price, B., Cohen, S., Brown, M.S.: When color constancy goes wrong: Correcting improperly white-balanced images. In: IEEE/CVF Conf. Comput. Vis. Pattern Recog. pp. 1535–1544 (2019)
7. Akazawa, T., Kinoshita, Y., Shiota, S., Kiya, H.: N-white balancing: White balancing for multiple illuminants including non-uniform illumination. IEEE Access **10**, 89051–89062 (2022)
8. Bach, M.: Color assimilation illusions (Last accessed: 03-10-2024), michaelbach.de/ot
9. Beigpour, S., Riess, C., Van De Weijer, J., Angelopoulou, E.: Multi-illuminant estimation with conditional random fields. IEEE Trans. Image Process. **23**, 83–96 (2013)
10. Bianco, S., Cusano, C.: Quasi-unsupervised color constancy. In: IEEE/CVF Conf. Comput. Vis. Pattern Recog. pp. 12212–12221 (2019)
11. Bianco, S., Cusano, C., Schettini, R.: Single and multiple illuminant estimation using convolutional neural networks. IEEE Trans. Image Process. **26**(9), 4347–4362 (2017)
12. Bianco, S., Schettini, R.: Color constancy using faces. In: IEEE Conf. Comput. Vis. Pattern Recog. pp. 65–72 (2012)
13. Blakeslee, B., McCourt, M.E.: A unified theory of brightness contrast and assimilation incorporating oriented multiscale spatial filtering and contrast normalization. Vision Res. **44**(21), 2483–2503 (2004)
14. Bleier, M., Riess, C., Beigpour, S., Eibenberger, E., Angelopoulou, E., Tröger, T., Kaup, A.: Color constancy and non-uniform illumination: Can existing algorithms work? In: IEEE Int. Conf. Comput. Vision Workshops. pp. 774–781 (2011)
15. Brainard, D.H., Freeman, W.T.: Bayesian method for recovering surface and illuminant properties from photosensor responses. In: Human Vision Vis. Process. Digit. Display V. vol. 2179, pp. 364–376. SPIE (1994)
16. Brainard, D.H., Freeman, W.T.: Bayesian color constancy. J. Opt. Soc. America A **14**(7), 1393–1411 (1997)
17. Brainard, D.H., Radonjic, A.: Color constancy. Vis. Neurosciences **1**, 948–961 (2004)
18. Buchsbaum, G.: A spatial processor model for object colour perception. J. Franklin Inst. **310**, 1–26 (1980)
19. Buzzelli, M., Zini, S., Bianco, S., Ciocca, G., Schettini, R., Tchobanou, M.K.: Analysis of biases in automatic white balance datasets and methods. Color Res. Appl. **48**(1), 40–62 (2023)
20. Cheng, D., Prasad, D.K., Brown, M.S.: Illuminant estimation for color constancy: Why spatial-domain methods work and the role of the color distribution. J. Opt. Soc. America A **31**, 1049–1058 (2014)
21. Corney, D., Lotto, R.B.: What are lightness illusions and why do we see them? PLoS Comput. Biol. **3**(9), e180 (2007)
22. Das, P., Liu, Y., Karaoglu, S., Gevers, T.: Generative models for multi-illumination color constancy. In: IEEE/CVF Conf. Comput. Vis. Pattern Recog. pp. 1194–1203 (2021)

23. Dayley, B., Dayley, D.: Adobe Photoshop CS6 Bible. John Wiley & Sons (2012)
24. Dixon, E.L., Shapiro, A.G.: Spatial filtering, color constancy, and the color-changing dress. J. Vision **17**(3), 7–7 (2017)
25. Domislović, I., Vršnak, D., Subašić, M., Lončarić, S.: One-net: Convolutional color constancy simplified. Pattern Recognit. Letters **159**, 31–37 (2022)
26. Ebner, M.: A parallel algorithm for color constancy. J. Parallel Distrib. Comput. **64**, 79–88 (2004)
27. Ebner, M.: Color Constancy, 1st ed. Wiley Publishing, ISBN: 0470058299 (2007)
28. Ebner, M.: Estimating the color of the illuminant using anisotropic diffusion. In: Int. Conf. Comput. Anal. Images Patterns. pp. 441–449 (2007)
29. Ebner, M.: Color constancy based on local space average color. Mach. Vision Appl. **20**(5), 283–301 (2009)
30. Ebner, M., Hansen, J.: Depth map color constancy. Bio-Algorithms and Med-Systems **9**(4), 167–177 (2013)
31. Emery, K.J., Webster, M.A.: Individual differences and their implications for color perception. Current Opinion Behavioral Sciences **30**, 28–33 (2019)
32. Ershov, E., Tesalin, V., Ermakov, I., Brown, M.S.: Physically-plausible illumination distribution estimation. In: IEEE/CVF Int. Conf. Comput. Vision. pp. 12928–12936 (2023)
33. Finlayson, G., Hordley, S.: Improving gamut mapping color constancy. IEEE Trans. Image Process. **9**(10), 1774–1783 (2000)
34. Finlayson, G.D., Hordley, S.D., Tastl, I.: Gamut constrained illuminant estimation. Int. J Comput. Vision **67**, 93–109 (2006)
35. Finlayson, G.D., Trezzi, E.: Shades of gray and colour constancy. In: Color and Imag. Conf. pp. 37–41. Society for Imaging Science and Technology (2004)
36. Forsyth, D.A.: A novel algorithm for color constancy. Int. J. Comput. Vision **5**(1), 5–35 (1990)
37. Foster, D.H., Nascimento, S.M.: Relational colour constancy from invariant cone-excitation ratios. Proc. Royal Soc. London. Ser. B: Biol. Sciences **257**(1349), 115–121 (1994)
38. Funt, B.V., Ciurea, F., McCann, J.J.: Retinex in matlab™. J. Electron. Imag. **13**(1) (2004)
39. Gao, S., Han, W., Yang, K., Li, C., Li, Y.: Efficient color constancy with local surface reflectance statistics. In: Eur. Conf. Comput. Vision. pp. 158–173. Springer (2014)
40. Gao, S., Zhang, M., Li, C., Li, Y.: Improving color constancy by discounting the variation of camera spectral sensitivity. J. Opt. Soc. America A **34**, 1448–1462 (2017)
41. Gao, S.B., Ren, Y.Z., Zhang, M., Li, Y.J.: Combining bottom-up and top-down visual mechanisms for color constancy under varying illumination. IEEE Trans. Image Process. **28**(9), 4387–4400 (2019)
42. Gao, S.B., Yang, K.F., Li, C.Y., Li, Y.J.: Color constancy using double-opponency. IEEE Transactions Pattern Anal. Mach. Intell. **37**(10), 1973–1985 (2015)
43. Gegenfurtner, K.R.: Reflections on colour constancy. Nature **402**(6764), 855–856 (1999)
44. Gegenfurtner, K.R.: Cortical mechanisms of colour vision. Nature Reviews Neuroscience **4**(7), 563–572 (2003)
45. Gehler, P.V., Rother, C., Blake, A., Minka, T., Sharp, T.: Bayesian color constancy revisited. In: IEEE Conf. Comput. Vis. Pattern Recog. pp. 1–8 (2008)
46. Gijsenij, A., Gevers, T., Van De Weijer, J.: Physics-based edge evaluation for improved color constancy. In: IEEE Conf. Comput. Vis. Pattern Recog. pp. 581–588 (2009)
47. Gijsenij, A., Gevers, T., Van De Weijer, J.: Generalized gamut mapping using image derivative structures for color constancy. Int. J. Comput. Vision **86**, 127–139 (2010)
48. Gijsenij, A., Gevers, T., Van De Weijer, J.: Improving color constancy by photometric edge weighting. IEEE Trans. Pattern Anal. Mach. Intell. **34**, 918–929 (2011)
49. Gijsenij, A., Lu, R., Gevers, T.: Color constancy for multiple light sources. IEEE Trans. Image Process. **21**(2), 697–707 (2011)

50. Gomez-Villa, A., Martín, A., Vazquez-Corral, J., Bertalmío, M.and Malo, J.: On the synthesis of visual illusions using deep generative models. J. Vision **22**(8), 2–2 (2022)
51. Gomez-Villa, A., Martin, A., Vazquez-Corral, J., Bertalmío, M.: Convolutional neural networks can be deceived by visual illusions. In: IEEE/CVF Conf. Comput. Vis. Pattern Recog. pp. 12309–12317 (2019)
52. He, K., Sun, J., Tang, X.: Guided image filtering. IEEE Trans. Pattern Anal. Machine Intell. **35**(6), 1397–1409 (2012)
53. Hirsch, E., Tal, A.: Color visual illusions: A statistics-based computational model. Advances Neural Inf. Process. Syst. **33**, 9447–9458 (2020)
54. Hu, Y., Wang, B., Lin, S.: Fc4: Fully convolutional color constancy with confidence-weighted pooling. In: IEEE/CVF Conf. Comput. Vis. Pattern Recog. (2017)
55. Hurlbert, A.: Colour constancy. Current Biology **17**(21), R906–R907 (2007)
56. Hussain, M.A., Akbari, A.S., Halpin, E.A.: Color constancy for uniform and non-uniform illuminant using image texture. IEEE Access **7**, 72964–72978 (2019)
57. Joze, H.R.V., Drew, M.S., Finlayson, G.D., Rey, P.A.T.: The role of bright pixels in illumination estimation. In: Color Imag. Conf. pp. 41–46. Society for Imaging Science and Technology (2012)
58. Kınlı, F., Yılmaz, D., Özcan, B., Kıraç, F.: Modeling the lighting in scenes as style for auto white-balance correction. In: IEEE/CVF Winter Conf. Appl. Comput. Vision. pp. 4903–4913 (2023)
59. Kubota, Y., Hiyama, A., Inami, M.: A machine learning model perceiving brightness optical illusions: Quantitative evaluation with psychophysical data. In: Proc. Augmented Humans Int. Conf. pp. 174–182 (2021)
60. Laakom, F., Raitoharju, J., Iosifidis, A., Nikkanen, J., Gabbouj, M.: Color constancy convolutional autoencoder. In: Symp. Ser. Comput. Intell. pp. 1085–1090. IEEE (2019)
61. Land, E.H.: The retinex theory of colour vision. Proc. Roy. Institution Gr. Britain **47**, 23–58 (1974)
62. Land, E.H.: The retinex theory of color vision. Scientific Amer. **237**, 108–129 (1977)
63. Land, E.H., McCann, J.J.: Lightness and retinex theory. J. Opt. Soc. America A **61**(1), 1–11 (1971)
64. Linnell, K.J., Foster, D.H.: Space-average scene colour used to extract illuminant information. John Dalton's Colour Vision Legacy pp. 501–509 (1997)
65. Luo, M.R., Cui, G., Rigg, B.: The development of the CIE 2000 colour-difference formula: CIEDE2000. Color Res. Appl. **26**, 340–350 (2001)
66. Marini, D., Rizzi, A.: A computational approach to color illusions. In: Int. Conf. Image Anal. Process. pp. 62–69. Springer (1997)
67. Marini, D., Rizzi, A.: A computational approach to color adaptation effects. Image Vision Comput. **18**(13), 1005–1014 (2000)
68. Mertens, T., Kautz, J., Van Reeth, F.: Exposure fusion. In: Pacific Conf. Comput. Graph. Appl. pp. 382–390. IEEE (2007)
69. Mitra, S., Mazumdar, D., Ghosh, K., Bhaumik, K.: An adaptive scale gaussian filter to explain white's illusion from the viewpoint of lightness assimilation for a large range of variation in spatial frequency of the grating and aspect ratio of the targets. PeerJ **6**, e5626 (2018)
70. Novick, D., Kitaoka, A.: The confetti illusion. J. Illusion **2** (2021)
71. Qian, Y., Kamarainen, J.K., Nikkanen, J., Matas, J.: On finding gray pixels. In: IEEE/CVF Conf. Comput. Vis. Pattern Recog. pp. 8062–8070 (2019)
72. Qian, Y., Pertuz, S., Nikkanen, J., Kämäräinen, J.K., Matas, J.: Revisiting gray pixel for statistical illumination estimation. In: Int. Joint Conf. Comput. Vision Imag. Comput. Graph. Theory Appl. vol. 4, pp. 36–46. INSTICC (2019)
73. Robinson, A.E., Hammon, P.S., de Sa, V.R.: Explaining brightness illusions using spatial filtering and local response normalization. Vision Res. **47**(12), 1631–1644 (2007)

74. Shapiro, A., Hedjar, L., Dixon, E., Kitaoka, A.: Kitaoka's tomato: two simple explanations based on information in the stimulus. i-Perception **9**(1), 2041669517749601 (2018)
75. Shapiro, A., Lu, Z.L.: Relative brightness in natural images can be accounted for by removing blurry content. Psychological Sci. **22**(11), 1452–1459 (2011)
76. Sharma, G., Wu, W., Dalal, E.N.: The CIEDE2000 color-difference formula: Implementation notes, supplementary test data, and mathematical observations. Color Res. Appl. **30**, 21–30 (2005)
77. Sheth, B.R., Young, R.: Two visual pathways in primates based on sampling of space: exploitation and exploration of visual information. Frontiers Integrative Neuroscience **10**, 37 (2016)
78. Shi, K., Luo, M.R., Rider, A.T., Song, S., Huang, T., Stockman, A.: Individual differences in color matches and cone spectral sensitivities in 51 young adults. Optics Express **32**, 23597–23616 (2024)
79. Song, A.and Faugeras, O., Veltz, R.: A neural field model for color perception unifying assimilation and contrast. PLoS Comput. Biol. **15**(6), e1007050 (2019)
80. Ulucan, O.: Color assimilation illusions (Last accessed: 08-10-2024), math-inf.uni-greifswald.de/institut/ueber-uns/mitarbeitende/oguzhan-ulucan/
81. Ulucan, O., Ulucan, D., Ebner, M.: BIO-CC: Biologically inspired color constancy. In: Brit. Mach. Vision Conf. BMVA Press (2022)
82. Ulucan, O., Ulucan, D., Ebner, M.: Color constancy beyond standard illuminants. In: IEEE Int. Conf. Image Process. pp. 2826–2830 (2022)
83. Ulucan, O., Ulucan, D., Ebner, M.: Block-based color constancy: The deviation of salient pixels. In: IEEE Int. Conf. Acoust. Speech Signal Process. pp. 1–5 (2023)
84. Ulucan, O., Ulucan, D., Ebner, M.: Multi-scale block-based color constancy. In: Eur. Signal Process. Conf. pp. 536–540. IEEE (2023)
85. Ulucan, O., Ulucan, D., Ebner, M.: Multi-scale color constancy based on salient varying local spatial statistics. The Vis. Comput. pp. 1–17 (2023)
86. Ulucan, O., Ulucan, D., Ebner, M.: Investigating color illusions from the perspective of computational color constancy. In: Int. Joint Conf. Comput. Vision Imag. Comput. Graph. Theory Appl. INSTICC (2024)
87. Van De Weijer, J., Gevers, T., Gijsenij, A.: Edge-based color constancy. IEEE Trans. Image Process. **16**, 2207–2214 (2007)
88. White, M.: A new effect of pattern on perceived lightness. Perception **8**(4), 413–416 (1979)
89. White, M.: The effect of the nature of the surround on the perceived lightness of grey bars within square-wave test gratings. Perception **10**(2), 215–230 (1981)
90. Yucer, K., Kim, C., Sorkine-Hornung, A., Sorkine-Hornung, O.: Depth from gradients in dense light fields for object reconstruction. In: Int. Conf. 3D Vision. IEEE (2016)
91. Zeki, S.: A Vision of the Brain. Blackwell Science, ISBN: 0632030545 (1993)
92. Zeman, A., Brooks, K.R., Ghebreab, S.: An exponential filter model predicts lightness illusions. Frontiers Human Neuroscience **9**, 368 (2015)
93. Zhang, X.S., Gao, S.B., Li, R.X., Du, X.Y., Li, C.Y., Li, Y.J.: A retinal mechanism inspired color constancy model. IEEE Trans. Image Process. **25**(3), 1219–1232 (2016)
94. Zuiderveld, K.: Contrast limited adaptive histogram equalization. Graph. Gems pp. 474–485 (1994)